NJC

Accepted Manuscript

This article can be cited before page numbers have been issued, to do this please use: D. R. Vinayakumara, K. Swamynathan, S. Kumar and A. V. Adhikari, *New J. Chem.*, 2019, DOI: 10.1039/C9NJ01192G.

ROYAL SOCIETY OF CHEMISTRY

rsc.li/njc

Columnar self-assembly of novel benzylidenehydrazones and their difluoroboron complexes: structure-property correlations

D. R. Vinayakumara,[a] K. Swamynathan,[b] Sandeep Kumar,[b] Airody Vasudeva Adhikari *[a]

[a] Organic Materials Laboratory, Department of Chemistry, National Institute of Technology Karnataka, Surathkal, Mangalore-575 025, India. E-mail: avachem@gmail.com; avachem@nitk.ac.in

[b] SCM group, Raman Research Institute, C.V. Raman Avenue, Sadashivanagar, Bangalore-560 080, India.

Abstract

Organoboron complexes are considered to be an important class of optically dynamic materials and because of their imperative properties, they have been unceasingly studied in a wide range of scientific areas. In this context, a new family of D-A-D′ architectured boron difluoride complexes **FB1-4** derived from arylhydrazones **HZ1-4** has been synthesized and characterized. The work also deliberates detailed studies on their thermal, self-assembling and optoelectronic properties with respect to structural modifications. The systematic studies reveal that, the new arylhydrazone ligands and their BF_2 complexes exhibit prospective columnar mesomorphism with different 2D lattice geometries at room temperature, owing to their critical structural features. Interestingly, an unusual morphological cross-over from columnar hexagonal to rectangular mesophase has been confirmed in one of the investigated pseudo-discoidal boron complexes, **FB4**. Their optoelectronic studies showcased their ICT dominating dye properties. Finally, the experimental results have been consciously correlated with quantum chemical simulations.

Introduction

Since the discovery, columnar self-assembly of disc-like molecules have attracted great scientific attention because of their potential utility in the wide range of electronic devices.[1–6] Typically, disc-like (discotic) or properly tailored non-discotic aromatic molecules are known to self-segregate into one-dimensional columnar stacking by the dint of various noncovalent interactions in the average intra- and inter-columnar spacings of 0.3-0.4 and 2-4 nm, respectively.[7] Due to this fact, discotic liquid crystals (DLCs) are considered as soft one-dimensional conducting molecular wires and they are identified to be better alternatives for the highly expensive organic single crystals or insulating amorphous conjugated polymers. In addition to their intrinsic charge transporting ability, they own inherent anisotropic photoconductivity, controlled molecular order, easy processability, good self-healing, excellent

optical absorption, intense fluorescence and great response to various external stimuli. These advantageous features render DLCs as promising candidates in several commercial applications.[8,9]

In recent years, enormous research is progressing in the design and development of functional DLCs to meet the basic demands for the individual device fabrication. As a result, a large variety of discotics have emerged in the last two decades. Particularly, discotic mesogens with preserved solid-state luminescence have been an emerging class of advanced optical materials for their promising candidature in organic light emitting diode (OLED), which is known to be a next generation eco-friendly lighting technology. Till date, many fluorescent columnar liquid crystalline (CLCs) materials have been investigated as potential emissive components in OLEDs.[10–17] One of the strategies to achieve luminescent CLC materials is the introduction of donor-accepter configuration to the core system. Evidently, organoboron complexes (OBCs) are imperious building blocks to achieve the highly fluorescent LC compounds. These OBCs provide easy access for a variety of structural modulations in order to tune for the desirable electro-optical properties.[18] Generally, OBCs can be divided into tri-coordinate and tetra-coordinate complexes, the latter complexes are known to be highly stable than the former one.[19] To construct the four-coordinated complexes, difluoroboron (BF_2) has been extensively used to lock configurationally in the three usual modes, *viz*. [O, O′],[20–22] [N, O] [23–26] and [N, N′]. [27–30] and these complexes were often derived from different chelating ligands such as α, β-diketonates,[31–34] β-diketiminates,[35,36] formazanates,[37–40] and quinolone-β-ketones.[41,42] Consequently, such complexes often possess remarkable thermal and photochemical stability; their low lying LUMO intensify the fluorescence; they have good electron transport ability. Hence, these metalloid complexes have been successfully employed in various electro-optical applications such as OLEDs, OFET, solar cells, photosensitizers, sensors, optical imaging and other. [18,19,43–45]

A number of BF_2 complexes with [N,N] and [O,O] chelating ligands have been reported as mesogenic fluorophores.[46–50] However, only two BF_2-[N,O] complexes were known, one with heterocyclic benzoxazoles [51] and the other with salicylideneamines ligands.[52] Yet, liquid crystalline BF_2 complexes from hydrazones have not been known. In continuing our research on luminescent columnar liquid crystals,[17,53,54] we explore a new series of columnar mesogenic boron difluoride complexes derived from benzylidenehydrazones for the first time. The new molecules comprise non-symmetrical conjugative attachment of alkoxyaryl groups to 2,2-difluoro-1,3,4,2-oxadiazaborol-3-ium-2-uide ring. The number and length of peripheral chains

of one of the arms were kept intact and both the functions were varied on the other arm. Their self-assembling, photophysical and electrochemical properties were studied as a function of the structural modifications. Interestingly, the key-precursors, *i.e.* non-symmetrical polycatenar arylhydrazones were also found to be mesomorphic. Finally, the report deals with the structure-property correlations of arylhydrazones and their BF_2 complexes with respect to their mesogenic and optoelectronic properties.

Results and discussion

Synthesis and characterization

The synthetic route for the preparation of polycatenar arylhydrazones (**HZ1-4**) and the corresponding difluoroboron complexes (**FB1-4**) is outlined in Scheme 1. The synthesis of key precursors, *i.e.* substituted arylhydrazones is often straightforward which involves simple acid catalyzed condensation of hydrazine derivative **H12** with different alkoxy substituted benzaldehydes (**A1-4**) by refluxing in ethanol for two hours. The hydrazine Schiff bases were purified by repeated recrystallization in methanol. The required aldehydes (**A1-4**) and phenylhydrazine (**H12**) were synthesized by adopting reported procedures with slight modifications and their synthetic pathway is summarized in Scheme S1.[55,56]

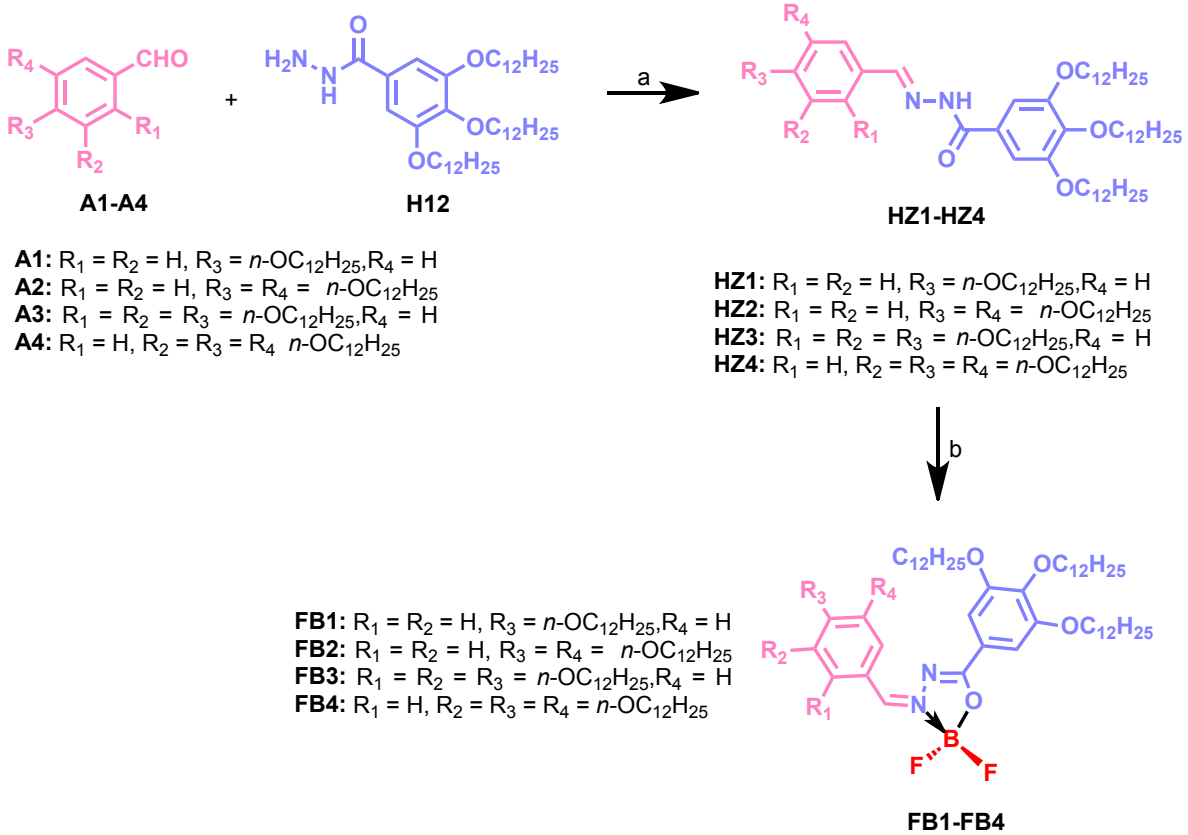

Scheme-1. Synthetic routes of new organoboron mesogens; reagents and conditions: (a) cat. AcOH, ethanol, 70 °C, 2 hrs, 69-75 %; (b) DIPEA, BF_3OEt_2, DCE, overnight, 42-60%

View Article Online
DOI: 10.1039/C9NJ01192G

The obtained new hydrazone derivatives, **HZ1-4** exist in keto-enol forms as shown in Scheme 2; the coordination with the boron source prefers the enolic tautomer form.[57] On boronation with boron trifluoride etherate in presence of *N,N*-Diisopropylethylamine, hydrazones yielded the corresponding difluoroboron complexes in 42-60%. The chemical structures of all key-precursors, and organoboron complexes were established using FTIR, ^{1}H-NMR ^{13}C-NMR spectral and elemental analyses; the associated structural data are furnished in supporting information.

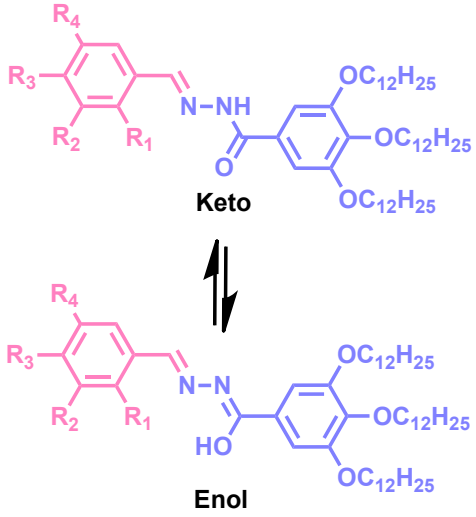

Scheme-2. Tautomer forms of new hydrazone derivatives

Thermal and self-assembling properties

The thermotropic phase behavior and the thermodynamic features of both hydrazones and boron complexes were studied by using Differential Scanning Calorimetry (DSC) and Polarized Optical Microscope (POM) techniques. The thermotropic phase transitions and their corresponding enthalpy changes are summarized in Table 1. Further, nature and symmetry of self-assembly were evaluated by the temperature variable wide-angle X-ray diffraction experiments.

Mesomorphism of benzylidenehydrazones (HZ1-4)

The DSC thermogram of first member of the series **HZ1** bearing four dodecyloxy peripheral chains displayed single reversible transition owing to crystal to isotropic transition without any mesomorphic behavior as depicted in Figure S31. In contrast, hydrazone **HZ2** with an increased number of alkyl chains exhibited an enantiotropic mesophase transition as evidenced by its DSC scan (Figure 1c). On heating cycle, it showed two distinct crystalline morphology and transformed into a mesophase (104.39 ℃) which clears at 145.5 ℃ with the

View Article Online
DOI: 10.1039/C9NJ01192G

energy change of 1.46 kJmol^{-1}. The observed phases were certainly reappeared in the cooling scan as well. These thermotropic transitions were further confirmed by POM; under cross polarizers, **HZ2** displayed a pseudo-focal conic fan-shaped texture with dark homeotropic regions and it crystallized below 92 ℃ as visualized in Figures 1a-b indicating the existence of optically uniaxial columnar phase.[58]

Table 1. [a] Phase transition temperatures (℃) and the corresponding energy changes (kJmol^{-1})

Compd.	Phase sequence	
	Heating	Cooling
HZ1	Cr 71.03 (82.076) I	I -14.39 (-6.14) Cr
HZ2	Cr_1 94.24 (54.50) Cr_2 104.39 (24.55) Col_h 145.50 (1.46) I	I 141.45 (-1.29) Col_h 92.01 (-24.79) Cr_2 82.29 (-59.91) Cr_1
HZ3	Cr 8.47 (23.67) Col_h 154.70 (2.74) I	150.44 (-2.94) Col_h 0.0 (-27.79) Cr
HZ4	Col_{h1} 93.59 (3.12) Col_{h2} 174.23 (13.79) I	I 171.70 (-12.26) Col_{h2} 92.25 (-2.66) Col_{h1} 0.13 (-37.40) Cr

[a] Peak temperatures/℃ (enthalpy/kJmol^{-1}) obtained by second heating and first cooling at the rate of 5 ℃/min; Col_h = Columnar hexagonal phase; I = Isotropic liquid phase

To get further insight into the nature of columnar assembly of **HZ2**, its X-ray diffraction patterns were obtained at various temperatures within the mesophase thermal region and they were found to be similar as shown in Figure 1d. For instance, a pattern gained at 135 ℃ showed a single reflection in its lower-angle region at the *d*-spacing of 23.0 Å, which could be indexed to (10) plane of hexagonal symmetry with lattice parameter a = 26.55 Å. Additionally, a noticed diffused halo in the wide-angle region at the maxima of 4.55 Å and the absence of core-core reflection manifested the fluidic property of the mesophase. In fact, the occurrence of single lower angle reflection can't elucidate the hexagonal lattice unambiguously. Nevertheless, this kind of patterns are commonly observed in various discotics. Indeed, the typical birefringent textural features strappingly confirm the Col_h mesophase. Further, the hexagonal lattice area, S and its volume, V were estimated to be 611 Å^2 and 2779 Å^3, respectively.

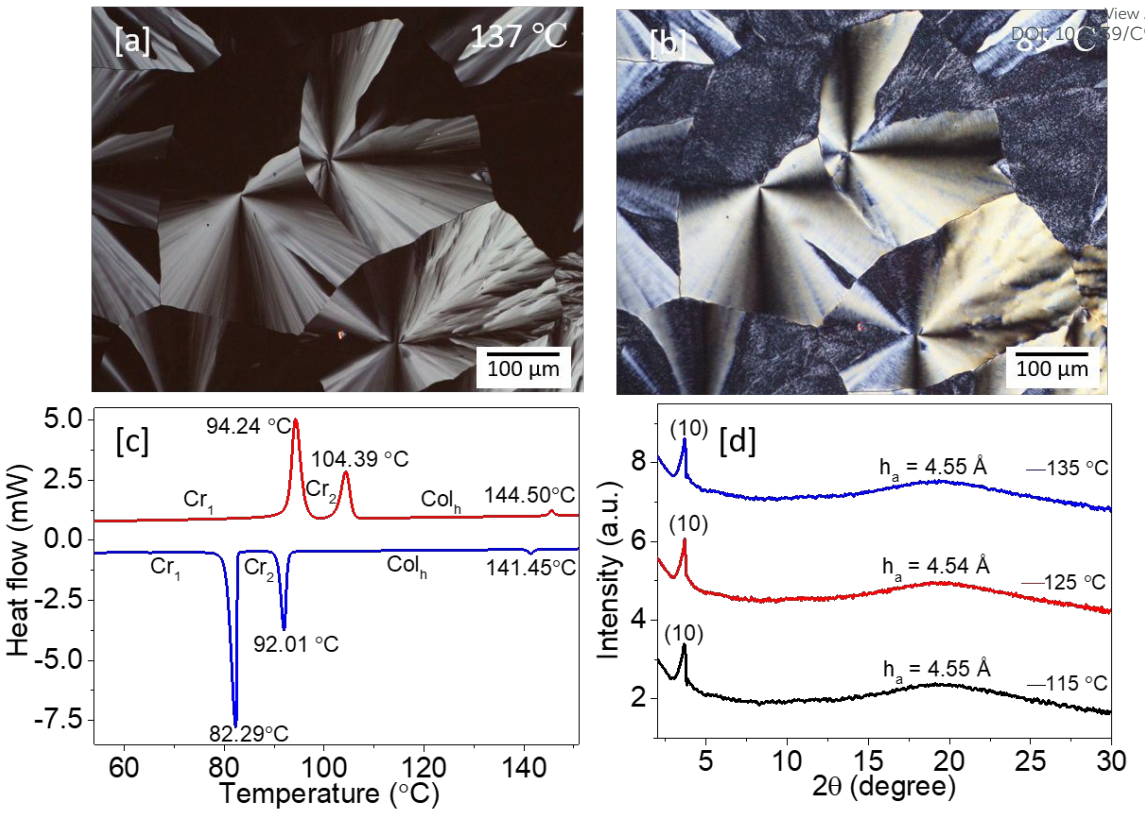

Figure 1. POM texture of **HZ2** at (a) 137 ℃ and (b) 85 ℃; (c) DSC thermogram of **HZ2** (red and blue traces represent heating and cooling scan, respectively); (d) XRD pattern of **HZ2** at various temperature points

The hexacatenar hydrazone, **HZ3** was easily be sheared between the two glass slides and it looked birefringent under POM indicating that, the compound is already in LC state at RT. Seemingly, the optical transitions were well consistent with its DSC results and it also exhibits the pseudo-focal conic texture on slow cooling below its isotropic temperature 150.44 ℃, confirming the columnar hexagonal mesophase (Figures 2a-c). As noticed in case of **HZ2**, the XRD patterns of **HZ3** also showed a single reflection at lower-angle region (23.90 Å at 55 ℃) with a wide-angle broad hump at 4.55 Å which is attributed to the fluidic assembly of alkyl chains as depicted in Figure 3a. The first intense peek can be indexed into a hexagonal lattice with a = 27.59 Å and the calculated mesophase parameters are summarized in Table 2. The compound **HZ4** behaves thermotropically different from **HZ3**, although they are regioisomeric derivatives. **HZ4** has two distinct mesophases with the isotropic transition at 174.23 ℃, which is the highest clearing temperature among the four investigated hydrazones and it shows crystallization at 0.13 ℃ on cooling below lower temperature phase (Figure 2d). As can be seen in Figures 2e-f, the material displayed fan type of texture below I phase, which on further cooling slight increase in brightness of the birefringent domains was realized. To identify the

symmetry of the columnar phase, XRD data were collected at the different temperatures in both higher and lower temperature mesophase ranges on cooling from its liquid phase. The patterns obtained in both the mesophase regions were apparently similar and their lower angle reflections were indexed to (10) plane of the hexagonal lattice (Figure 3b). To differentiate between these two mesophases, we named lower temperature mesophase as Col_{h1} and Col_{h2} for higher temperature mesophase, since there is a clear thermodynamic transition with considerable enthalpy change (3.12 kJmol^{-1}) associated with it. This kind of transition is frequently observed in compounds with non-discoidal molecular geometry.

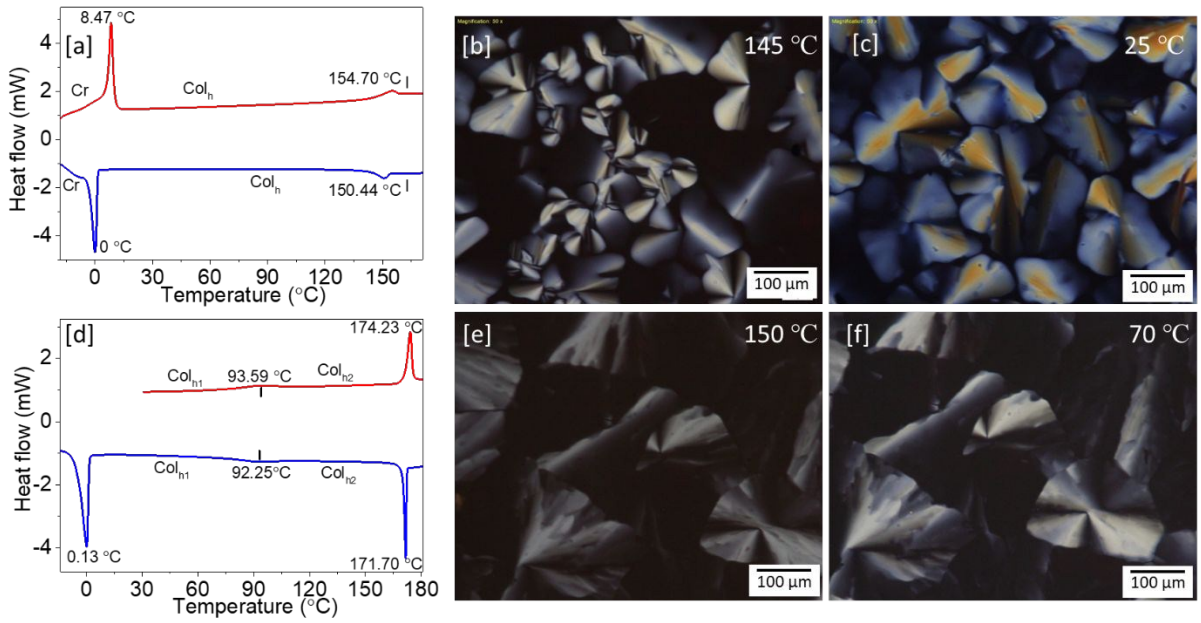

Figure 2. (a) DSC thermogram of **HZ3** (red and blue traces represent heating and cooling scan, respectively); POM texture of **HZ3** captured at (b) 145 °C and (c) 25 °C; (d) DSC thermogram of **HZ4** (red and blue traces represent heating and cooling scan, respectively); POM texture of **HZ4** at (e) 150 °C and (f) 70 °C

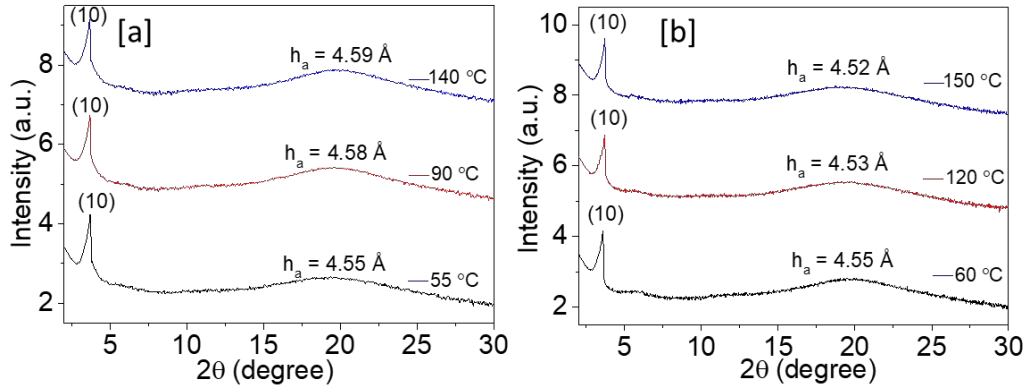

Figure 3. (a) XRD pattern obtained for Col_h phase of **HZ3** and (b) Col_{h1} and Col_{h2} phases of **HZ4** at various temperatures

To understand the possible molecular packing in these hydrazone derivatives, the number of molecules accompanied per each columnar stratum Z was calculated by assuming the density ρ = 1 g cm^{-3}. [59] Subsequently, the Z was found to be 1.5, 1.35 and 1.4 for **HZ2**, **HZ3** and **HZ4**, respectively. The observed non-integral values suggest that, there may be folding and/or intercalation of peripheral tails in the columnar cross-section. It is reported that, this kind of benzylidenehydrazones stabilize the columnar phase by the formation of helical superstructures wherein the H-bonded chain of N-H···O=C adopts a helical conformation. Because of this reason, they embrace more than one molecules per columnar unit in order to maintain the average circular cross-section for organizing in a hexagonal lattice.[58]

Table 2. XRD data of new hydrazones

Compd.	Phase (T/°C)	d_{obs} (Å)	d_{cal} (Å)	Miller Indices (hk)	Lattice parameter a (Å), Lattice area S (Å^2), Molecular volume V (Å^3)
HZ2	Col_h (135)	23.0 4.55 (h_a)	23.0	(10)	a = 26.55 S = 610.83 V = 2779.3 Z = 1.46
HZ3	Col_h (55)	23.90 4.55 (h_a)	23.90	(10)	a = 27.59 S = 659.6 V = 3001.1 Z = 1.35
HZ4	Col_{h1} (60)	24.67 4.43(h_a)	24.67	(10)	a = 28.48 S = 702.76 V = 3113.23 Z = 1.40
HZ4	Col_{h2} (150)	23.82 4.56(h_a)	23.82	(10)	a = 27.50 S = 655.16 V = 2992.0 Z = 1.35

d_{obs} , experimental lattice spacing; d_{cal}, calculated from the lattice parameter, a for the hexagonal lattice; h_a, alkyl chains correlation peak value; h_c, core-core spacing; Z, number of molecules per columnar slice; S, lattice area; V, molecular volume

View Article Online
DOI: 10.1039/C9NJ01192G

Mesomorphism of boron difluoride complexes (FB1-4)

The thermotropic phase behavior of all the boron difluoride complexes was also investigated systematically. Evidently, upon coordination with BF_2 the mesomorphism of hydrazones **HZ1-4** was completely altered. The thermal phase sequence and corresponding thermodynamic parameters of **FB1-4** are tabulated in Table 3. The first member of the series bearing four alkyl tails was crystalline in nature, it melted at the same temperature (~71.0 ℃) as its ligand **HZ1**. However, the enthalpy change for the melting transition of **FB1** was found to be much higher than **HZ1** indicating the greater thermal stability of $\mathbf{BF_1}$ complex in the solid state (Figure S32). Unlike **HZ2**, its boron complex **FB2** was characterized to be non-mesogenic, instead it showed three distinct crystalline morphology as evidenced by its DSC thermogram (Figure S33). The non-mesomorphism of **FB2** may be due to the lack of space occupation by only five alkyl chains around the central aromatic segment. While its ligand molecules (**HZ2**) segregated into columnar phase because of co-operative intermolecular hydrogen bonding as discussed earlier.

Table 3. [a] Phase transition temperatures (℃) and the corresponding energy changes ($kJmol^{-1}$)

Compd.	Phase sequence	
	Heating	Cooling
FB1	Cr 71.25 (71.91) I	I -14.39 (-54.36) Cr
FB2	Cr_1 44.19 (14.31) Cr_2 66.83 (10.57) Cr_3 96.98 (50.45) I	I 86.50 (-52.19) Cr_3 61.99 (-9.14) Cr_2 41.48 (-12.44) Cr_1
FB3	Cr_1 10.48 (7.39) Cr_2 31.03 (23.92) Col_h 35.01 (0.62) I	I 32.08 (-1.09) Col_h 2.20 (-22.10) Cr
FB4	Col_h 66.19 (23.83) Col_r 96.65 (15.82) I	I 87.78 (-15.97) Col_r 61.11 (-23.61) Col_h

[a] Peak temperatures/℃ (enthalpy/$kJmol^{-1}$) obtained by second heating and first cooling at the rate of 5 ℃/min; Col_r = Columnar rectangular phase; Col_h = Columnar hexagonal phase; I = Isotropic liquid phase

The two regioisomers, **FB3** and **FB4** bearing six peripheral chains exhibit entirely different thermotropic phase transitions from each other. The isomer **FB3** having dodecyloxy chains at 2nd, 3rd and 4th positions shows a trivial endothermic transition at 35.01 ℃ (ΔH = 0.62 $kJmol^{-1}$) which could be assigned to an LC to I transformation. On cooling scan, the transition

occurred at 32.08 °C (ΔH = -1.09 kJmol^{-1}) and the phase gets crystallized at 2.20 °C as shown in Figure 4a. The perceived mosaic pattern was the typical indication of presence of columnar mesomorphism (Figures 4b-c).

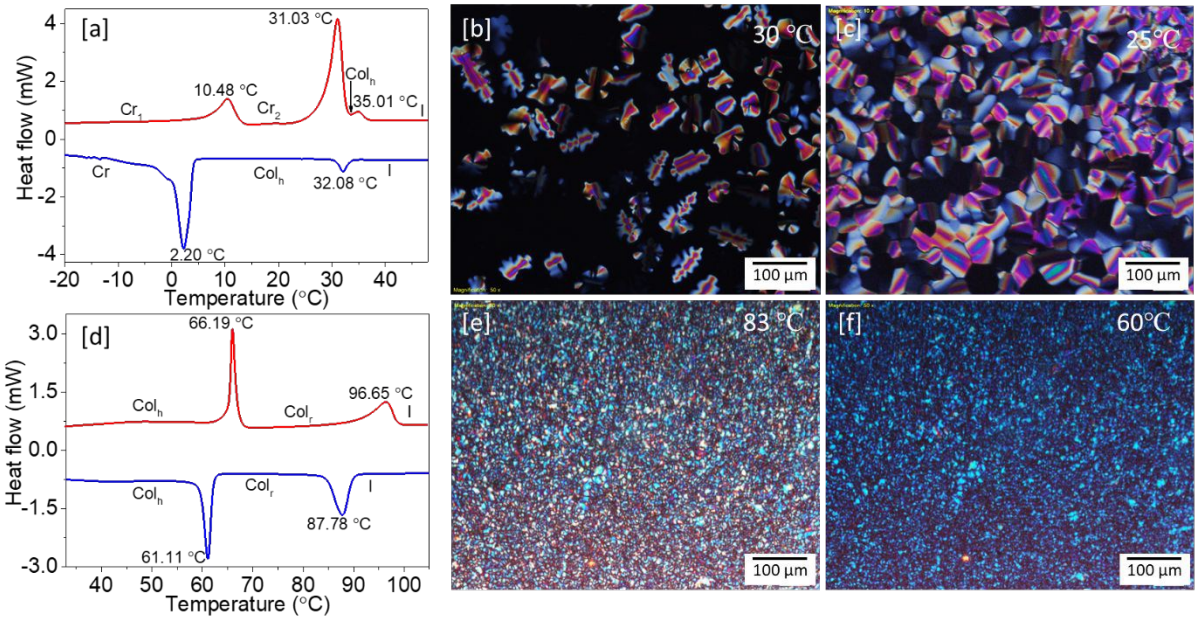

Figure 4. (a) DSC thermogram of **FB3** (red and blue traces represent heating and cooling scan, respectively); POM texture of **FB3** captured at (b) 30 °C and (c) 25 °C; (d) DSC thermogram of **FB4** (red and blue traces represent heating and cooling scan, respectively); POM texture of **FB4** at (e) 83 °C and (f) 60 °C

Further, XRD pattern of **FB3** confirms the hexagonal lattice structure with the lattice parameter a = 28.39 Å (Figure 5a). Whereas, its isomeric derivative **FB4** having dodecyloxy chains at 3rd, 4th and 5th positions exhibited two distinct enantiotropic mesophases as demonstrated in DSC trace (Figure 4d). It displayed two reversible transitions with slightly larger enthalpy values (ΔH = 24 kJmol^{-1} for LC-LC and ΔH = 16 kJmol^{-1} for LC-I). The observed ΔH is much higher than that of its isomer **FB3**, this could be due to the compact arrangement of **FB4** in the mesophase. These results reveal that, changing the position of the peripheral chains in the non-discoidal molecules significantly stabilizes the mesophase. The lower temperature phase of **FB4** was assigned to Col$_h$ mesophase (Figure 5b). A number of XRD reflections in the lower-angle region at higher temperature mesophase have been indexed to a centre rectangular columnar geometry with space group symmetry of *C2mm* as the peak indexation follows the extinction rule $h+k$ = even number (Figure 5c). The unit cell parameters calculated from the diffraction pattern are a = 30.34 A and b = 62.38 A. This unusual transition from hexagonal to rectangular columnar results in doubling of the lattice volume and hence the number of constituent molecules also doubles in each unit cell. This kind of hexagonal to

rectangular phase transition was previously observed in case of triphenylene derivatives.[60] Based on the XRD results, we propose a model to demonstrate the self-assembly of **FB4** molecules as illustrated in Figure 6.

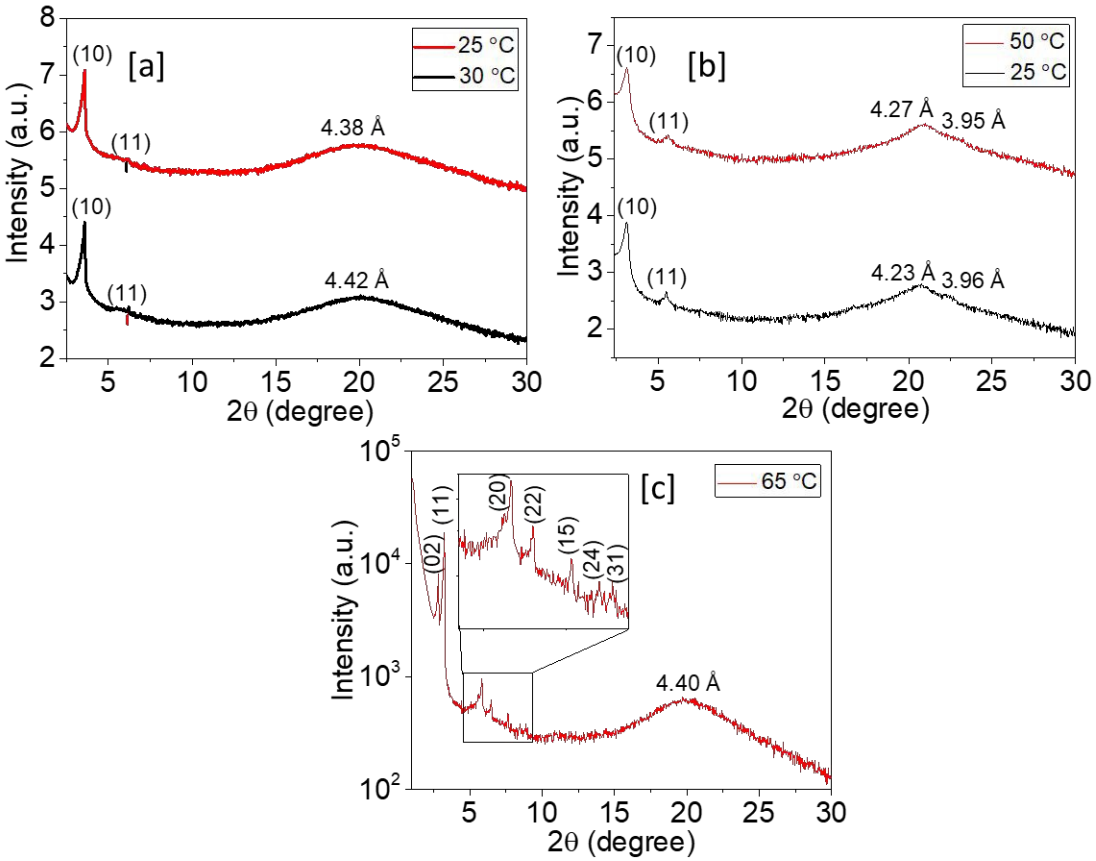

Figure 5. XRD pattern obtained for (a) Col_h phase of **FB3**; XRD traces recorded within (b) lower and (c) high-temperature mesophase ranges of **FB4**

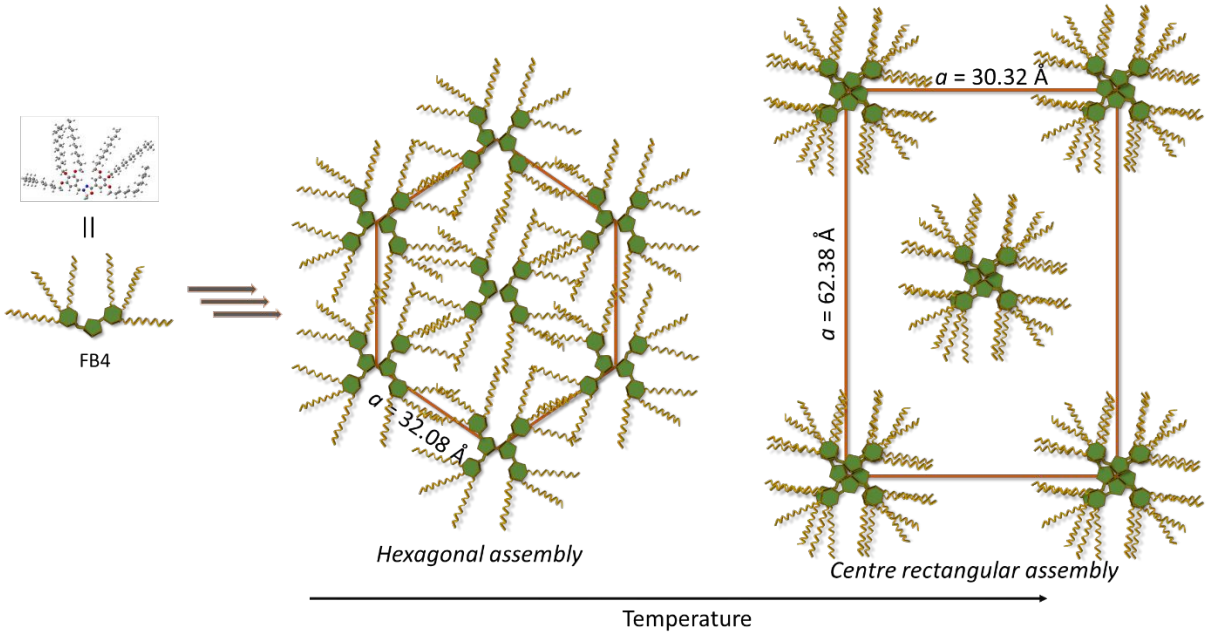

Figure 6. Schematic illustration of phase transition of **FB4**

Table 4. XRD characterization data of new organoboron complexes

Compounds	Phase (T/°C)	d_{obs} (Å)	d_{cal} (Å)	Miller Indices (hk)	Lattice parameter a (Å), Lattice area S (Å^2), Molecular volume V (Å^3)
FB3	Col_h (27)	24.59	24.59	(10)	a = 28.39
		14.26	14.19	(11)	S = 698.2
		4.42 (h_a)			V = 3086.1
					Z = 1.34
FB4	Col_h (25)	28.24	28.24	(10)	a = 32.08
		16.04	16.30	(11)	S = 920.0
		4.23 (h_a)			V = 3646.7
		3.96 (h_c)			Z = 1.73
	Col_r (65)	31.19	31.19	(02)	a = 30.32
		27.27	27.27	(11)	b = 62.38
		15.15	15.16	(20)	S = 1891.7
		13.61	13.63	(22)	V = 8322.0
		11.56	11.53	(15)	Z = 3.60
		10.42	10.87	(24)	
		9.95	9.97	(31)	
		4.40 (h_a)			

d_{obs} ,d_{cal}, are observed and calculated value of d spacings. Lattice parameter, a for the hexagonal lattice; h_a, alkyl chains correlation peak value; h_c, core-core spacing; Z, number of molecules per unit cell; S, lattice area; V, molecular volume

Photophysical studies

The optical properties of newly synthesized D-A-D′ configured boron difluoride complexes were studied by recording their steady-state absorption and emission spectra in DCM solution ($c = 2\times10^{-5}$ M) at room temperature. The obtained spectra are depicted in Figure 7a-b, and the subsequent key parameters are summarized in Table 5. Seemingly, a variation in number of alkoxy chains has the least influence on their absorption property; whereas they exert a slight impact on their emission behavior. In their absorption spectra, the observed higher energy bands at ~230 nm are due to localized π-π* electronic transition of alkoxyphenyl rings and the intense longer wavelength bands (377-385 nm) are assigned to delocalized intramolecular charge transfer (ICT) transitions from π (D) to π* (A) of the molecules. On

exciting at their absorption maxima, they show single featureless broad emission bands indicating the floppy nature of the excited state.[61] Their emission maxima were noticed in the range of 492-524 nm; interestingly, **FB1** bearing four alkoxy donors displayed red-shifted emission compared to **FB2** and **FB3** having five and six respective alkoxy substitutions, respectively. This may be related to the structural reorganization of the molecules in the excited state. Certainly, they exhibit larger Stokes shift in the range of 5514 -7331 cm^{-1} confirming the pronounced ICT behavior of these unsymmetrical dyad systems and the property is one of the key factors in the fabrication of OLED devices. Further, to understand the emission behavior of the complexes in the solid state, the PL spectra were recorded for their drop-casted thin films and the resulting spectra are shown in Figure 7c. Evidently, they showed blue-shifted emission maxima when compared to their respective peaks in solution. The fact may be due to the H-type aggregation of the molecules in the solid state. Furthermore, the optical band gap values of these materials were estimated by considering red-edge of their respective absorption spectrum and they were found to in the range of 2.81-2.90 eV.

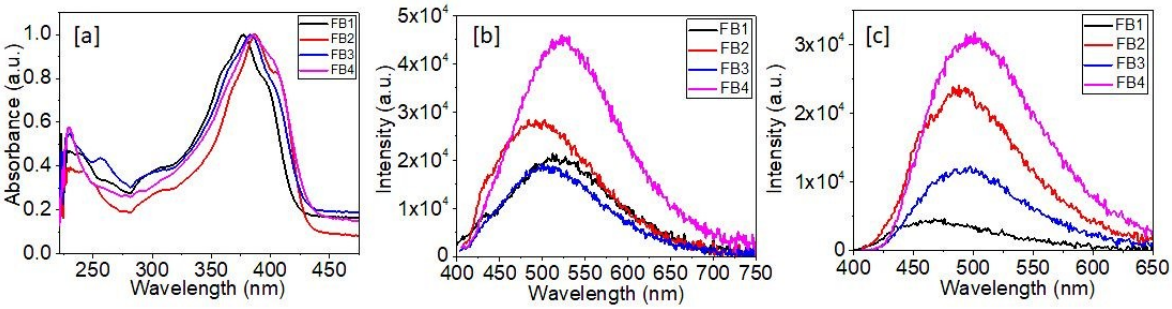

Figure 7. (a) UV-Visible absorption and (b) photoluminescence spectra of **FB1-4** at $c = 2\times10^{-5}$ M DCM solution; (c) drop-casted thin film photoluminescence spectra of **FB1-4**

Table 5. Photophysical characterization data of new complexes

Compd.	[a] λ_{abs} (nm)	[a] λ_{em} (nm)	Stokes shift (cm^{-1})	[a b] $E_{g\ opt}$ (eV)	[c] λ_{em} (nm)
FB1	228, 377	521	7331	2.90	468
FB2	228, 387	492	5514	2.85	488
FB3	230, 384	508	6357	2.84	494
FB4	230, 385	524	6890	2.81	501

[a] Determined form DCM solution at $c = 2\times10^{-5}$ M, [b] Optical band gap estimated by red edge of absorption band in UV-visible spectrum, [c] Estimated for thin films

Theoretical studies

The Density Functional Theory (DFT) calculations were performed for all the new complexes to establish their structure-property correlation. The calculations were accomplished using Gaussian 09 software by means of Becke's three-parameter functions hybridized with the Lee-Yang-Par functional and the 6-31G (d,p) basis set. The geometries of all complexes were optimized under vacuum condition and computed energy minimized structures are showcased in Figures 8a-b. As visualized in Figure 8b, central core-system comprising three rings adopts entirely planar geometry which fundamentally helps for the stabilization of columnar arrangement. Further, the alkyl chains surrounded by this planar core moiety facilitate to acquire more or less disc-shaped molecules.

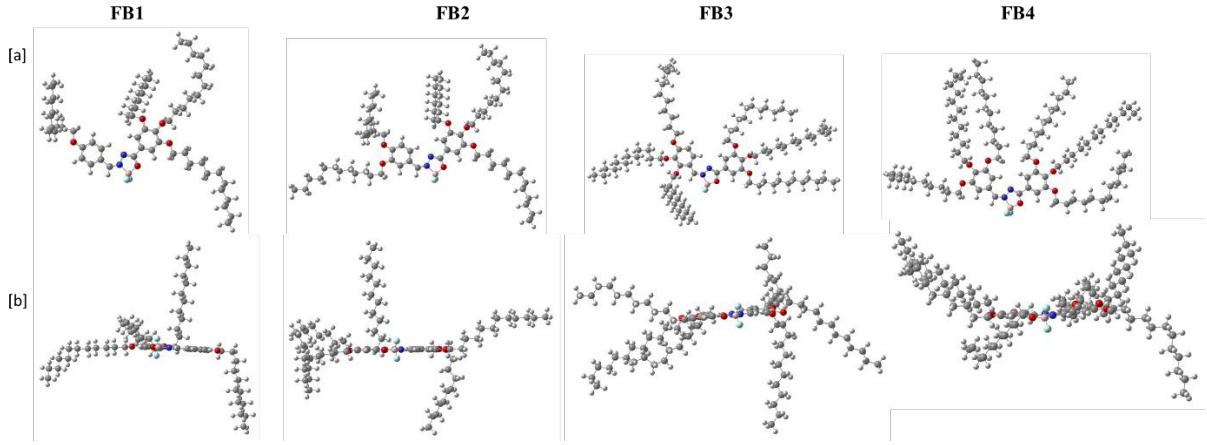

Figure 8. (a) Energy minimized structures of new BF_2 complexes and (b) their side view

The electronic distributions in the frontier molecular orbitals (FMOs) are displayed in Figure 9 and the simulated electrochemical data are tabulated in Table 6. The HOMOs are localized over the two alkoxyphenyl rings with a slight contribution from the boron-containing central core. Contrary, LUMOs are concentrated on the central ring and the alkoxyphenyl ring attached through imine linkage. The results clearly indicate the electronic migration from the donor to acceptor units, which manifests the ICT behaviour of the complexes. The observed fact has reflected in experimental absorption spectral measurements. The simulated HOMO and LUMO energy levels were found to be in the range of -5.56 to 5.69 and -2.02 to -2.21 eV, respectively. The calculated energy bang gap (E_g) was noticed to be slightly higher than that of the optical band gap. However, the trend of E_g is in good agreement with the experimental values.

View Article Online
DOI: 10.1039/C9NJ01192G

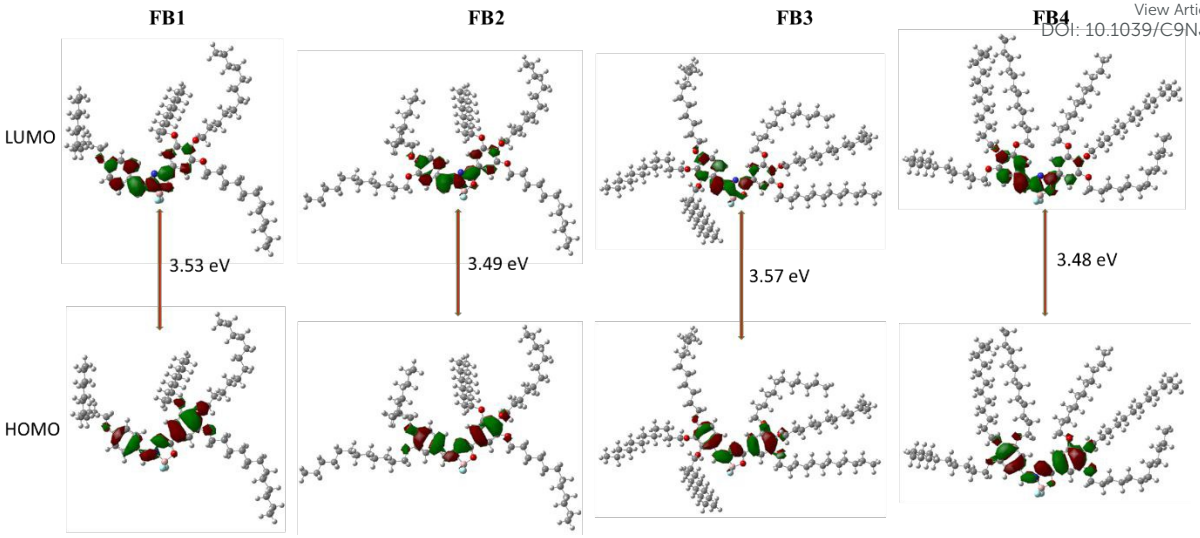

Figure 9. Electronic distributions in the FMOs of new BF_2 complexes

Table 6.[a] Theoretical electrochemical data of new complexes

Compd.	HOMO (eV)	LUMO (eV)	[a]$E_{g\ DFT}$ (eV)	[b]$E_{g\ Opt}$ (eV)
FB1	-5.665	-2.136	3.529	2.90
FB2	-5.565	-2.078	3.487	2.85
FB3	-5.598	-2.027	3.571	2.84
FB4	-5.695	-2.212	3.483	2.81

[a]The values obtained in DFT calculations to vacuum; [b] optical band gap obtained by UV-visible spectra

Conclusion

In summary, we have designed and synthesized a novel series of organoboron complexes (**FB1-4**) featuring dyad structural motif with a critical chain length. They were subjected to in-depth liquid crystalline and optoelectronic studies. Interestingly, the key-precursors benzylidenehydrazones (**HZ1-4**) exhibited columnar mesophase with the hexagonal structure mainly by means of co-operative intermolecular hydrogen bonding, at ambient conditions. Contrary, their corresponding BF_2 complexes showed different thermotropic phase behaviour. The mesomorphic properties of these hemi-discoidal boron complexes are greatly dependent on number and position of fluidic chains around the aromatic-core. Consequently, the isomeric complexes **FB3** and **FB4** displayed dissimilar thermotropic phase behaviour and showed distinct columnar mesophase at different temperature ranges. Their experimental optoelectronic studies as well as theoretical simulations explored their significant ICT behavior. Conclusively, these prospective π-conjugated materials possessing stable Col phase would be the promising candidates for molecular electronic applications.

Conflicts of interest

There are no conflicts of interest to declare.

Acknowledgement

The authors are thankful to NITK, Surathkal and SCM group, RRI, Bangalore, India for providing necessary laboratory facilities. The authors are also thankful to Dr Vijayaraghavan for recording the NMR spectra and Mrs. N. Vasudha for their technical support. We are grateful to Prof. V. A. Raghunathan for his valuable inputs on XRD analysis. VK is grateful to NITK for providing fellowship.

References

1 S. Laschat, A. Baro, N. Steinke, F. Giesselmann, C. Haegele, G. Scalia, R. Judele, E. Kapatsina, S. Sauer and A. Schreivogel, *Angew. Chem. Int. Ed.*, 2007, **46**, 4832–4887.

2 V. Lemaur, D. A. da Silva Filho, V. Coropceanu, M. Lehmann, Y. Geerts, J. Piris, M. G. Debije, A. M. van de Craats, K. Senthilkumar and L. D. A. Siebbeles, *J. Am. Chem. Soc.*, 2004, **126**, 3271–3279.

3 S. Sergeyev, W. Pisula and Y. H. Geerts, *Chem. Soc. Rev.*, 2007, **36**, 1902–1929.

4 B. R. Kaafarani, *Chem. Mater.*, 2010, **23**, 378–396.

5 S. Kumar, *NPG Asia Mater.*, 2014, **6**, e82.

6 T. Wöhrle, I. Wurzbach, J. Kirres, A. Kostidou, N. Kapernaum, J. Litterscheidt, J. C. Haenle, P. Staffeld, A. Baro and F. Giesselmann, *Chem. Rev.*, 2015, **116**, 1139–1241.

7 A. Gowda, M. Kumar and S. Kumar, *Liq. Cryst.*, 2017, **44**, 1990–2017.

8 M. Kumar, A. Gowda and S. Kumar, *Part. Part. Syst. Charact.*, 2017, **34**, 1700003.

9 S. Kumar, *Chemistry of discotic liquid crystals: from monomers to polymers*, CRC press, 2016.

10 A. P. Sivadas, D. S. Rao, N. S. Kumar, D. D. Prabhu, S. Varghese, C. N. Ramachandran, R. M. Ongungal, S. Krishna Prasad and S. Das, *J. Phys. Chem. B*, 2017, **121**, 1922–1929.

11 J. De, S. P. Gupta, S. Sudheendran Swayamprabha, D. K. Dubey, I. Bala, I. Sarkar, G. Dey, J.-H. Jou, S. Ghosh and S. K. Pal, *J. Phys. Chem. C*, 2018, **122**, 23659–23674.

12 X. Wu, G. Xie, C. P. Cabry, X. Xu, S. J. Cowling, D. W. Bruce, W. Zhu, E. Baranoff and Y. Wang, *J. Mater. Chem. C*, 2018, **6**, 3298–3309.

13 I. Bala, L. Ming, R. A. K. Yadav, J. De, D. K. Dubey, S. Kumar, H. Singh, J.-H. Jou, K. Kailasam and S. K. Pal, *ChemistrySelect*, 2018, **3**, 7771–7777.

14 R. K. Gupta, D. Das, M. Gupta, S. K. Pal, P. K. Iyer and A. S. Achalkumar, *J. Mater. Chem. C*, 2017, **5**, 1767–1781.

15 Y. Wang, Y. Liao, C. P. Cabry, D. Zhou, G. Xie, Z. Qu, D. W. Bruce and W. Zhu, *J. Mater. Chem. C*, 2017, **5**, 3999–4008.

16 A. K. Yadav, B. Pradhan, H. Ulla, S. Nath, J. De, S. K. Pal, M. N. Satyanarayan and A. S. Achalkumar, *J. Mater. Chem. C*, 2017, **5**, 9345–9358.

17 D. R. Vinayakumara, H. Ulla, S. Kumar, A. Pandith, M. N. Satyanarayan, D. S. Rao, S. K. Prasad and A. V. Adhikari, *J. Mater. Chem. C*. 2018, **6**, 7385-7399.

18 D. Li, H. Zhang and Y. Wang, *Chem. Soc. Rev.*, 2013, **42**, 8416–8433.

19 K. Tanaka and Y. Chujo, *NPG Asia Mater.*, 2015, **7**, e223.

20 K. Ono, K. Yoshikawa, Y. Tsuji, H. Yamaguchi, R. Uozumi, M. Tomura, K. Taga and K. Saito, *Tetrahedron*, 2007, **63**, 9354–9358.

21 A. D'Aléo and F. Fages, *Photochem. Photobiol. Sci.*, 2013, **12**, 500–510.

22 M. Mamiya, Y. Suwa, H. Okamoto and M. Yamaji, *Photochem. Photobiol. Sci.*, 2016, **15**, 928–936.

23 R. S. Singh, M. Yadav, R. K. Gupta, R. Pandey and D. S. Pandey, *Dalton Trans.*, 2013, **42**, 1696–1707.

24 R. Yoshii, A. Nagai, K. Tanaka and Y. Chujo, *Macromol. Rapid Commun.*, 2014, **35**, 1315–1319.

25 K. Benelhadj, J. Massue and G. Ulrich, *New J. Chem.*, 2016, **40**, 5877–5884.

26 M.-J. Kwak and Y.-M. Kim, *Bull. Korean Chem. Soc.*, 2009, **30**, 2865–2866.

27 X. Zhang, H. Yu and Y. Xiao, *J. Org. Chem.*, 2011, **77**, 669–673.

28 W. Li, W. Lin, J. Wang and X. Guan, *Org. Lett.*, 2013, **15**, 1768–1771.

29 T. M. H. Vuong, J. Weimmerskirch-Aubatin, J.-F. Lohier, N. Bar, S. Boudin, C. Labbe, F. Gourbilleau, H. Nguyen, T. T. Dang and D. Villemin, *New J. Chem.*, 2016, **40**, 6070–6076.

30 M.-C. Chang and E. Otten, *Chem. Commun.*, 2014, **50**, 7431–7433.

31 E. Cogné-Laage, J.-F. Allemand, O. Ruel, J.-B. Baudin, V. Croquette, M. Blanchard-Desce and L. Jullien, *Chem. Eur. J.*, 2004, **10**, 1445–1455.

32 X. Zhang, R. Lu, J. Jia, X. Liu, P. Xue, D. Xu and H. Zhou, *Chem. Commun.*, 2010, **46**, 8419–8421.

33 C. Ran, X. Xu, S. B. Raymond, B. J. Ferrara, K. Neal, B. J. Bacskai, Z. Medarova and A. Moore, *J. Am. Chem. Soc.*, 2009, **131**, 15257–15261.

34 D.-J. Wang, B.-P. Xu, X.-H. Wei and J. Zheng, *J. Fluor. Chem.*, 2012, **140**, 49–53.

35 S. M. Barbon, V. N. Staroverov, P. D. Boyle and J. B. Gilroy, *Dalton Trans.*, 2014, **43**, 240–250.

36 F. P. Macedo, C. Gwengo, S. V. Lindeman, M. D. Smith and J. R. Gardinier, *Eur. J. Inorg. Chem.*, 2008, **2008**, 3200–3211.

37 M.-C. Chang, A. Chantzis, D. Jacquemin and E. Otten, *Dalton Trans.*, 2016, **45**, 9477–9484.

38 S. M. Barbon, V. N. Staroverov and J. B. Gilroy, *J. Org. Chem.*, 2015, **80**, 5226–5235.

39 S. M. Barbon, J. T. Price, P. A. Reinkeluers and J. B. Gilroy, *Inorg. Chem.*, 2014, **53**, 10585–10593.

40 M. Hesari, S. M. Barbon, V. N. Staroverov, Z. Ding and J. B. Gilroy, *Chem. Commun.*, 2015, **51**, 3766–3769.

41 R. Tan, Q. Lin, Y. Wen, S. Xiao, S. Wang, R. Zhang and T. Yi, *CrystEngComm*, 2015, **17**, 6674–6680.

42 Y. Kubota, H. Hara, S. Tanaka, K. Funabiki and M. Matsui, *Org. Lett.*, 2011, **13**, 6544–6547.

43 Q.-D. Liu, M. S. Mudadu, R. Thummel, Y. Tao and S. Wang, *Adv. Funct. Mater.*, 2005, **15**, 143–154.

44 Y.-L. Rao and S. Wang, *Inorg. Chem.*, 2011, **50**, 12263–12274.

45 P.-Z. Chen, L.-Y. Niu, Y.-Z. Chen and Q.-Z. Yang, *Coord. Chem. Rev.*, 2017, **350**, 196–216.

46 Y.-W. Chen, Y.-C. Lin, H.-M. Kuo and C. K. Lai, *J. Mater. Chem. C*, 2017, **5**, 5465–5477.

47 H. Maeda, Y. Terashima, Y. Haketa, A. Asano, Y. Honsho, S. Seki, M. Shimizu, H. Mukai and K. Ohta, *Chem. Commun.*, 2010, **46**, 4559–4561.

48 Y. Bando, S. Sakamoto, I. Yamada, Y. Haketa and H. Maeda, *Chem. Commun.*, 2012, **48**, 2301–2303.

49 I. Sánchez, C. Núñez, J. A. Campo, M. R. Torres, M. Cano and C. Lodeiro, *J. Mater. Chem. C*, 2014, **2**, 9653–9665.

50 Y. Haketa, S. Sasaki, N. Ohta, H. Masunaga, H. Ogawa, N. Mizuno, F. Araoka, H. Takezoe and H. Maeda, *Angew. Chem.*, 2010, **122**, 10277–10281.

51 Y.-W. Chen, G.-H. Lee and C. K. Lai, *Dalton Trans.*, 2017, **46**, 12274–12283.

52 Z.-Y. Lei, G.-H. Lee and C. K. Lai, *J. Mol. Liq.*, 2018, **260**, 44–56.

53 D. R. Vinayakumara, K. Swamynathan, S. Kumar and A. V. Adhikari, *New J. Chem.,* 2018, **42**, 16999-17008

54 D. R. Vinayakumara, H. Ulla, S. Kumar, M. N. Satyanarayan and A. V. Adhikari, *Mater. Chem. Front.*, 2018, **2**, 2297-2306

View Article Online
DOI: 10.1039/C9NJ01192G

55 S. Maruyama, K. Sato and H. Iwahashi, *Chem. Lett.*, 2010, **39**, 714–716.
56 G. Shanker and C. V. Yelamaggad, *New J. Chem.*, 2012, **36**, 918–926.
57 C. K. Lai, C. Tsai and Y. Pang, *J. Mater. Chem.*, 1998, **8**, 1355–1360.
58 G. Shanker, M. Prehm, C. V. Yelamaggad and C. Tschierske, *J. Mater. Chem.*, 2011, **21**, 5307–5311.
59 J. Tang, R. Huang, H. Gao, X. Cheng, M. Prehm and C. Tschierske, *RSC Adv.*, 2012, **2**, 2842–2847.
60 A. M. Levelut, *J. Chim. Phys.*, 1983, **80**, 149–161.
61 R. K. Konidena, K. J. Thomas, M. Singh and J.-H. Jou, *J. Mater. Chem. C*, 2016, **4**, 4246–4258.

View Article Online
DOI: 10.1039/C9NJ01192G

Table of Contents

A series of prospective columnar liquid crystalline materials derived from novel organoboron complexes has been developed in virtue of their application in organic electronic applications.